

Tensor Density Estimator by Convolution-Deconvolution

Yifan Peng¹, Siyao Yang^{*2}, Yuehaw Khoo³, and Daren Wang⁴

^{1,2}Committee on Computational and Applied Mathematics, University of Chicago

³Committee on Computational and Applied Mathematics and Department of Statistics,
University of Chicago

⁴Department of Applied and Computational Mathematics and Statistics, University of
Notre Dame

Abstract

In high-dimensional density estimation problems, most classical distance metrics between probability distributions suffer from the exponential growth of variance with respect to the dimensionality. In this paper, we propose a novel distance metric that avoids this curse of dimensionality based on a specifically chosen kernel. By matching the empirical density in terms of this metric, a low-rank tensor-train representation can be computed with a complexity that is linear in both sample size and dimensionality. It consists of three simple steps: convolving the empirical distribution with the kernel; compressing the empirical distribution after convolution as a tensor-train, with efficient tensor decomposition algorithms; and finally, applying a deconvolution to such a tensor-train representation. Numerical results demonstrate the high accuracy and efficiency of the proposed methods.

1 Introduction

Density estimation is a fundamental problem in data science with wide-ranging applications in fields such as science (Cranmer (2001); Chen (2017)), engineering (Chaudhuri et al. (2014)), and economics (Zambom and Dias (2013)). More precisely, given N data points $\{x^{(i)}\}_{i=1}^N \sim p^*$, where each $x^{(i)}$ is an independent and identically distributed (i.i.d.) sample from an unknown ground truth distribution $p^* : \mathbb{R}^d \rightarrow \mathbb{R}$, the goal is to estimate p^* based on empirical distribution

$$\hat{p}(x) = \frac{1}{N} \sum_{i=1}^N \delta_{x^{(i)}}(x) \quad (1)$$

where $\delta_{x^{(i)}}(x)$ is the Dirac delta function centered at $x^{(i)}$.

The concept of distance between two probability density functions is a crucial topic in the density estimation framework, especially for high-dimensional cases. However, most choices of distance have difficulty in accurately measuring the variance error $\text{Dist}(\hat{p}, p^*)$ in high dimensions due to the ‘‘curse of dimensionality’’, meaning that $\text{Dist}(\hat{p}, p^*)$ will grow exponentially fast with dimensionality d . Consequently, an exponential growth in sample size N is required in order for

*Corresponding author

an accurate measurement of variance error, making high-dimensional data analysis unaffordable. Such examples include the standard Euclidean distance (L_2 distance) (Aggarwal et al. (2001)), Wasserstein distances (Niles-Weed and Rigollet (2022); Weed and Bach (2019)) and the Kullback-Leibler (KL) divergence (Mardia et al. (2020)). Therefore, we need to develop a new notion of distance measure with moderate sample complexity that scales more favorably with respect to dimensionality.

In this paper, we propose a new distance metric for two probability density functions p, p' induced by certain non-standard kernel $K : \mathbb{R}^d \times \mathbb{R}^d \rightarrow \mathbb{R}$:

$$\text{Dist}_K(p, p') := \|p - p'\|_K = \|K(p - p')\|_{L_2}. \quad (2)$$

Here we slightly abuse the notation by treating K as an operator acting on a density function $(Kp)(x) := \int K(x, x')p(x')dx'$. With the new distance (2), density estimation can then be framed as solving the following optimization problem within a chosen function space \mathcal{F} :

$$\tilde{p} = \arg \min_{p \in \mathcal{F}} \text{Dist}_K(p, \hat{p}). \quad (3)$$

The new distance enjoys a variance that does not grow exponentially with the dimension, which is a necessary condition for the success of estimation. Furthermore, the restriction to a restrictive function class \mathcal{F} has a denoising effect, i.e. \tilde{p} cannot fit to noise.

The optimization problem (3) can be challenging to solve in general, depending on the parametrization within the space \mathcal{F} . In this paper, we consider \mathcal{F} as a low-rank functional tensor-train (TT) space, which allows us to solve the optimization efficiently using numerical linear algebra techniques. In short, we first convolve \hat{p} with the kernel as $K\hat{p}$, then we apply singular value decomposition based tensor decomposition algorithms to $K\hat{p}$ to get a low-rank TT. Finally, we perform a deconvolution with K^{-1} . Our approach is fundamentally different from classical iterative algorithms for (3), which are prone to getting trapped into local minima due to highly non-convex optimization landscape in high-dimensional cases.

1.1 Related work

Density estimation literature. Classical density estimation methods such as histograms (Scott (1979, 1985)), kernel density estimators (Parzen (1962); Davis et al. (2011)) and nearest neighbor density estimates (Mack and Rosenblatt (1979)) are known for their statistical stability and numerical robustness in low-dimensional cases. But they often struggle with the curse of dimensionality, even in moderately high-dimensional spaces. More recently, deep generative modeling has emerged as a powerful tool for generating new samples, particularly in the context of image, based on neural network architecture. This approach includes energy-based models (Kim and Bengio (2016); Du and Mordatch (2019); Song and Ermon (2019)) generative adversarial networks (GANs) (Goodfellow et al. (2020); Liu et al. (2021)), normalizing flows (Dinh et al. (2014); Rezende and Mohamed (2015); Dinh et al. (2016)), and autoregressive models (Germain et al. (2015); Uria et al. (2016); Papamakarios et al. (2017)). While the numerical performance for these modern methods is impressive, statistical guarantees and non-convex optimization convergence analysis remain challenging areas of research. Furthermore, for some of these models (e.g. energy based model), generating i.i.d. samples can still be expensive. For methods like GANs, while it can generate samples efficiently, it does not provide a way to evaluate the value of a density at any given point.

In short, it is difficult for a method to enjoy all the desirable properties such as easy to train, easy to generate samples, can support evaluation of density values, and can be estimated without the curse of dimensionality.

Tensor train from partial sensing of a function. Tensor train, also known as the matrix product state (MPS) (White (1993); Perez-Garcia et al. (2006)) in the physics literature, has recently been used when to uncover a function, when only limited number of observations of this function are given. Methods for this include TT-cross (Oseledets and Tyrtyshnikov (2010)), DMRG-cross (Savostyanov and Oseledets (2011)), TT completion (Liu et al. (2012); Song et al. (2019)), and others (Sun et al. (2020); Kressner et al. (2023); Shi et al. (2023)). It has broad applications in high-dimensional scientific computing problems (Kressner and Uschmajew (2016); Bachmayr et al. (2016) and machine learning (Stoudenmire and Schwab (2016); Huggins et al. (2019); Sengupta et al. (2022)).

Tensor train for density estimation. In a density estimation setting, we are not given observed entries of a density function, but just an empirical distribution of it. The key challenge lies in the randomness of the observed object, i.e. the empirical histogram, which contains an exponentially large variance in terms of the dimensionality. Therefore, reducing variance in a high-dimensional setting is crucial to design effective algorithms. Recently, work (Hur et al. (2023)) and subsequent studies (Tang et al. (2022); Peng et al. (2023); Chen and Khoo (2023); Tang and Ying (2023); Khoo et al. (2024)) employ sketching techniques in tensor decomposition step for density estimation problems, which originates from randomized linear algebra literature. However, most existing algorithms in these works do not have a general way to ensure a linear computational complexity when sketching, in terms of dimensionality. Another approach for density estimation with tensors is through optimization-based method. Works (Bradley et al. (2020); Han et al. (2018); Novikov et al. (2021)) implement gradient descent methods and optimize tensor-network representations according to some loss functions. However, the performance strongly depends on the initialization and often suffers from the problem of local minima due to the highly non-convex nature of the optimization landscape. Furthermore, these iterative procedures require multiple iterations over N data points, resulting in higher computational complexity compared to the previous tensor decomposition algorithms.

1.2 Contributions

Here we list our contributions:

1. **New distance metric without curse of dimensionality.** We introduce a new distance for high-dimensional density estimation. This distance is induced by a appropriately selected kernel such that its variance does not suffer from the curse of dimensionality.
2. **Algorithms for density estimation.** With the new distance metric, the density estimator \tilde{p} is obtained in a tensor-train representation by minimizing $\|\tilde{p} - \hat{p}\|_K$ by our proposed tensor compression algorithms which only use linear algebra. For the first time, we establish an algorithmic connection between two popular compressed representations: hierarchical matrix and tensor-train representation. In particular, hierarchical matrix is used to compress density moments, and these moments are used to sketch the tensor-train representation. We also proposed various other methods based on tensorized sketching and Nyström approximation to speed up the classical TT-SVD for density estimation. Several of these proposed methods

achieve a computational complexity of $O(dN)$ where d is the dimensionality and N is the sample size.

1.3 Organization

Here we summarize the organization of the paper. In Section 1.4, we introduce the tensor notation and the tensor diagram used frequently in the paper. In Section 2, we outline our approach, where the main component is to perform SVD efficiently on a specific tensor train. Section 3 includes an algorithm that utilizes the Nyström approximation to further accelerate the algorithm in Section 2. In Section 4, we study an algorithm that performs SVD efficiently by truncating the elements in the tensor, and then introduce a further acceleration by employing a hierarchical matrix factorization. Section 5 proposes an algorithm utilizing sketching matrix with a low-rank tensor structure. All of these different algorithms aim to reduce the computational complexity following different approaches. In Section 6, we showcase the comprehensive numerical results to demonstrate the high accuracy and efficiency for our proposed algorithms. Finally, in Section 7, we summarize our findings.

1.4 Tensor notation and tensor diagram

We begin with some definitions regarding tensors. A d -dimensional tensor $A \in \mathbb{R}^{n_1 \times n_2 \times \dots \times n_d}$ is a collection of entries denoted by $A(i_1, i_2, \dots, i_d)$ with $1 \leq i_j \leq n_j$ for $1 \leq j \leq d$. Diagrammatically, a tensor can be denoted as a node whose dimensionality is indicated by the number of the “legs” of the node. In Figure 1(a), the diagrams for a three-dimensional tensor A and a two-dimensional matrix B are plotted as an example. We use i_1, i_2, i_3 to denote the three legs in tensor A . We may also use a rectangle to denote a tensor when it has many legs in this paper.

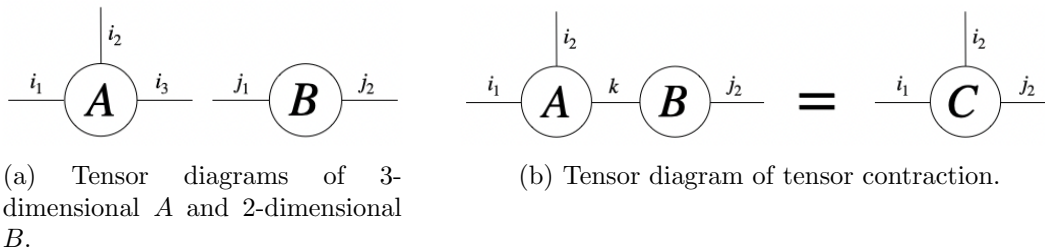


Figure 1: Basic tensor diagrams and operations.

Based on the definition of tensor, we list several tensor operations that will be used frequently in the paper:

1. **“ \circ ” contraction.** We use \circ to represent the tensor cores contraction $(A \circ B)(i_1, i_2, j_2) = \sum_k A(i_1, i_2, k)B(k, j_2)$. Such operation is denoted as diagram in Figure 1 (b) which combines the last leg of A and the first leg of B . The resulting $C = A \circ B$ is a three-dimensional tensor.
2. **Unfolding matrix.** Given a d -dimensional tensor with entries $A(i_1, i_2, \dots, i_d)$, if we group the first j indices into a multi-index $i_{1:j}$ and group the rest into another multi-index $i_{j+1:d}$, we will obtain a j -th unfolding matrix $A^{(j)} \in \mathbb{R}^{(n_1 \dots n_j) \times (n_{j+1} \dots n_d)}$ satisfying

$$A^{(j)}(i_{1:j}, i_{j+1:d}) = A(i_1, i_2, \dots, i_d). \quad (4)$$

In general, the memory cost of a high-dimensional tensor suffers from curse of dimensionality. Tensor-train representation is a way to decompose the whole exponential large d -dimensional tensor with underlying low-rank structure into d number of components:

$$A = G_1 \circ G_2 \circ \dots \circ G_d \in \mathbb{R}^{n_1 \times \dots \times n_d} \quad (5)$$

where $G_1 \in \mathbb{R}^{n_1 \times r_1}$, $G_2 \in \mathbb{R}^{r_1 \times n_2 \times r_2}$, \dots , $G_{d-1} \in \mathbb{R}^{r_{d-2} \times n_{d-1} \times r_{d-1}}$, $G_d \in \mathbb{R}^{r_{d-1} \times n_d}$ are called tensor cores and $\{r_j\}_{j=1}^{d-1}$ are the ranks. The TT representation can be visualized as the left panel of Figure 2. In addition, we use \mathcal{F}_c to denote the space of TT

$$\mathcal{F}_c = \left\{ G_1 \circ G_2 \circ \dots \circ G_d \text{ where } G_1 \in \mathbb{R}^{n_1 \times r_1}, G_2 \in \mathbb{R}^{r_1 \times n_2 \times r_2}, \dots, G_d \in \mathbb{R}^{r_{d-1} \times n_d} \right\}. \quad (6)$$

Throughout the paper, we denote the largest rank by

$$r = \max_j r_j.$$

Then the memory cost for storing A in TT form is at $O(dnr^2)$, which has no curse of dimensionality if r is small.

In addition, a TT can also be used to represent a continuous function formulated as a tensor product basis function expansion. We use the notation \mathcal{F} to represent the space of such functional tensor trains, which is given by

$$\mathcal{F} = \left\{ p \left| p(x_1, x_2, \dots, x_d) = \sum_{l_1, l_2, \dots, l_d=1}^n A(l_1, l_2, \dots, l_d) \phi_{l_1}(x_1) \phi_{l_2}(x_2) \dots \phi_{l_d}(x_d), \right. \right. \\ \left. \left. \text{where } \{\phi_l\}_{l=1}^n \text{ are univariate basis functions and coefficient } A = G_1 \circ G_2 \circ \dots \circ G_d \in \mathcal{F}_c \right\}.$$

The functional tensor-train representation is illustrated in the right panel of Figure 2.

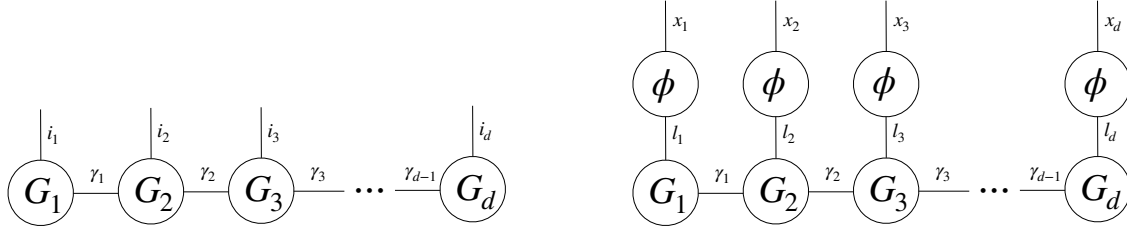


Figure 2: Diagram for tensor-train representation. Left: discrete case. Right: continuous case.

2 Main approach

In this section, we sketch the framework of our main approach. The goal is to get the density estimator \tilde{p} that approximates given empirical distribution \hat{p} via the optimization problem

$$\tilde{p} = \arg \min_{p \in \mathcal{F}} \|p - \hat{p}\|_K. \quad (7)$$

To solve it, we consider a proper choice of kernel K with decomposition

$$K(x, x') = \Phi(x)\text{diag}(\alpha)\Phi(x')^T \quad (8)$$

where $\Phi(x) = [\Phi_l(x)]_l$ is a row vector of a chosen orthonormal basis $\{\Phi_l\}_l$ evaluated on x and α are the corresponding weights associated with each basis. In what follows, we regard

$$\Phi := [\Phi_l(x)]_{x,l}$$

as a matrix with row indexed by x and columns indexed by l . With this notation, the kernel operator K is formulated as

$$K = \Phi\text{diag}(\alpha)\Phi^T.$$

Our main approach to solve (7) can be summarized as the following three steps:

1. **Convolution.** Project the empirical distribution \hat{p} to “coefficients” \hat{c} under certain basis expansion:

$$\hat{c} = \text{diag}(\alpha)\Phi^T\hat{p} = \text{diag}(\alpha) \int \Phi(x)^T \hat{p}(x) dx. \quad (9)$$

2. **Tensor compression.** Approximate \hat{c} as a TT \tilde{c} .

3. **Deconvolution.** Get the desired density estimator based on the TT coefficient \tilde{c} :

$$\tilde{p} = \Phi\text{diag}(\alpha)^{-1}\tilde{c}. \quad (10)$$

\tilde{p} is also a TT, if $\Phi\text{diag}(\alpha)^{-1}$ has an appropriate low-rank tensor structure.

To understand why the three steps above solve the optimization problem (7), we notice that with the choice of kernel (8), the introduced distance (2) in the function space is equivalent to the Frobenius distance in the coefficient space:

$$\|p - p'\|_K^2 = \|K(p - p')\|_{L_2}^2 = \|\text{diag}(\alpha)\Phi^T(p - p')\|_F^2 \quad (11)$$

for any $p, p' \in \mathcal{F}$. The last equality holds due to the orthonormality of basis function Φ . With notation $\hat{c} = \text{diag}(\alpha)\Phi^T\hat{p}$, we have

$$\min_{p \in \mathcal{F}} \|p - \hat{p}\|_K^2 = \min_{p \in \mathcal{F}} \|\text{diag}(\alpha)\Phi^T p - \hat{c}\|_F^2. \quad (12)$$

In order to obtain p in TT format, a simple way is to first compress \hat{c} as a TT \tilde{c} , and then we solve

$$\min_{p \in \mathcal{F}} \|\text{diag}(\alpha)\Phi^T p - \tilde{c}\|_F^2 \quad (13)$$

which is done by the deconvolution step of the proposed method.

In the rest of this section, we will further elaborate each step with details. In Section 2.1, we discuss the choice of the kernel. In Section 2.2, we explain one tensor decomposition algorithm and its fast implementation for density estimation setting. In Section 2.3, we demonstrate some details on how to implement kernel deconvolution.

2.1 Kernel choice

In this subsection, we discuss the choice of kernel K . Without loss of generality, we assume the domain of interest in this work to be the hypercube $\Omega = [-1, 1]^d$. The kernel is assumed to be a product of univariate kernel:

$$K(x, x') = K_1(x_1, x'_1)K_2(x_2, x'_2) \cdots K_d(x_d, x'_d) \quad \text{where} \quad K_j(x_j, x'_j) = \sum_{l_j=1}^n \alpha_{l_j} \phi_{l_j}(x_j) \phi_{l_j}(x'_j). \quad (14)$$

where $\{\phi_l\}_{l=1}^n$ are certain chosen orthogonal basis function and is assumed to be bounded by 1, i.e.,

$$\|\phi_l\|_{L_\infty(\Omega)} \leq 1 \quad \text{for all } l = 1, \dots, n, \quad (15)$$

which is satisfied by many choices of orthogonal basis functions including Fourier basis, Legendre polynomial basis, etc. Under such setting, $\text{diag}(\alpha)$ and $\Phi(x)$ in (8) are respectively given by

$$\text{diag}(\alpha) = \bigotimes_{j=1}^d \text{diag}(\alpha_1, \alpha_2, \dots, \alpha_n), \quad \Phi(x) = \bigotimes_{j=1}^d [\phi_1(x_j), \phi_2(x_j), \dots, \phi_n(x_j)]. \quad (16)$$

Next, we elaborate the choice of eigenvalues $\{\alpha_l\}_{l=1}^n$ in the kernel (14). In particular, $\{\alpha_l\}_{l=1}^n$ should be properly chosen such that the introduced distance $\|p - p'\|_K$ can avoid the curse of dimensionality. By (15) and the normalization condition for probability density functions, the distance in (11) can be bounded by

$$\begin{aligned} \|p - p'\|_K^2 &= \sum_{l_1, \dots, l_d=1}^n \alpha_{l_1}^2 \cdots \alpha_{l_d}^2 \left[\int \cdots \int (p(x) - p'(x)) \left(\prod_{j=1}^d \phi_{l_j}(x_j) \right) dx \right]^2 \\ &\leq \sum_{l_1, \dots, l_d=1}^n \alpha_{l_1}^2 \cdots \alpha_{l_d}^2 \|p - p'\|_{L_1(\Omega)}^2 \prod_{j=1}^d \|\phi_{l_j}\|_{L_\infty(\Omega)}^2 \\ &\leq \sum_{l_1, \dots, l_d=1}^n 4\alpha_{l_1}^2 \cdots \alpha_{l_d}^2 = 4(\alpha_1^2 + \alpha_2^2 + \cdots + \alpha_n^2)^d. \end{aligned} \quad (17)$$

Note that when $\alpha_l \equiv 1$, $\|\cdot\|_K$ reduces to $\|\cdot\|_{L_2}$ and will grow exponentially with dimensionality from the above estimation. To avoid such curse of dimensionality, we choose α_l satisfying $\alpha_1^2 + \alpha_2^2 + \cdots + \alpha_n^2 \leq 1 + \frac{C}{d}$ for some constant C without d dependency, then the distance is bounded without curse of dimensionality:

$$\|p - p'\|_K^2 \leq 4\left(1 + \frac{C}{d}\right)^d \leq 4\exp(C). \quad (18)$$

In this paper, we choose $\{\alpha_l\}_{l=1}^n$ as

$$\alpha_l = \begin{cases} 1, & l = 1; \\ \alpha, & l = 2, \dots, n. \end{cases} \quad (19)$$

By setting $\alpha = O(\frac{1}{\sqrt{nd}})$, $\|p - p'\|_K$ will not increase exponentially in terms of dimensionality. However, we point out that α should not be chosen to be too small, which might lead to instability in our later operations. This will be further elaborated in Section 2.3.

2.2 Tensor-train SVD (TT-SVD)

In this subsection, we focus on Step 2 of main approach — tensor compression. To this end, we propose to use the Tensor-train SVD (TT-SVD) algorithm. The TT-SVD algorithm is originally proposed in [Oseledets \(2011\)](#), which compresses a high-dimensional tensor into a low-rank tensor train by performing truncated singular value decomposition (SVD) sequentially. For our problem, we use TT-SVD to find the best low-rank approximation \tilde{c} of \hat{c} . Given samples $\{x^{(i)}\}_{i=1}^N$, by (9), \hat{c} is formulated as

$$\hat{c} = \frac{1}{N} \sum_{i=1}^N \tilde{\Phi}_1^{(i)} \otimes \tilde{\Phi}_2^{(i)} \otimes \dots \otimes \tilde{\Phi}_d^{(i)} \quad (20)$$

where $\tilde{\Phi}_j^{(i)} = [\alpha_1 \phi_1(x_j^{(i)}), \alpha_2 \phi_2(x_j^{(i)}), \dots, \alpha_n \phi_n(x_j^{(i)})] \in \mathbb{R}^n$.

This expression is plotted as tensor diagrams in Figure 3. In addition, we use $\tilde{\Phi}_j \in \mathbb{R}^{N \times n}$ to denote the matrix whose rows are $\tilde{\Phi}_j^{(i)}$ for future use. Then \tilde{c} in TT format that approximates \hat{c}

$$\hat{c} = \frac{1}{N} \sum_{i=1}^N \tilde{\Phi}_1^{(i)} \otimes \tilde{\Phi}_2^{(i)} \otimes \dots \otimes \tilde{\Phi}_d^{(i)}$$

Figure 3: Tensor diagram of \hat{c} .

can be obtained following the procedures in Algorithm 1.

Algorithm 1 TT-SVD

INPUT: Tensor $\hat{c} \in \mathbb{R}^{n \times n \times \dots \times n}$. Target rank $\{r_1, \dots, r_{d-1}\}$.

- 1: **for** $j \in \{1, \dots, d-1\}$ **do**
- 2: Perform SVD to $B_j \in \mathbb{R}^{nr_{j-1} \times n^{d-j}}$, which is formed by the following tensor contraction

$$B_j = \hat{G}_1 \otimes \dots \otimes \hat{G}_{j-1} \otimes \hat{c}$$

In particular, $B_1 = \hat{c}^{(1)}$ which is the first unfolding matrix of \hat{c} defined in (4). With SVD $B_j = U_j \Sigma_j V_j^T$, we obtain the j -th core $\hat{G}_j \in \mathbb{R}^{r_{j-1} \times n \times r_j}$, which is reshaped from the first r_j principle left singular vectors in U_j .

3: **end for**

4: Obtain the last core $\hat{G}_d = B_d \in \mathbb{R}^{r_{d-1} \times n}$.

OUTPUT: Tensor train $\tilde{c} = \hat{G}_1 \circ \hat{G}_2 \circ \dots \circ \hat{G}_d \in \mathbb{R}^{n \times n \times \dots \times n}$.

Below, we briefly outline the idea behind this algorithm. When $j = 1$, we want to obtain the first core \hat{G}_1 by performing SVD to $\hat{c}^{(1)}$ (which is B_1 in Algorithm 1). Then we let $\hat{G}_1 \in \mathbb{R}^{n \times r_1}$ to be first r_1 principle left singular vectors. The rationale of the first step is to approximate $\hat{c}^{(1)}$ as $\hat{c}^{(1)} \approx \hat{G}_1 (\hat{G}_1^T \hat{c}^{(1)})$. In the $j = 2$ step, we want to obtain \hat{G}_2 , which gives a further approximation to $\hat{G}_1 (\hat{G}_1^T \hat{c}^{(1)})$. The way we do this is to factorize $\hat{G}_1^T \hat{c}^{(1)} \in \mathbb{R}^{r_1 \times n^{d-1}}$, by applying SVD to B_2 ,

which is the reshaping of $\hat{G}_1^T \hat{c}^{(1)}$. This completes the $j = 2$ step. Then we do the above procedure recursively till $j = d - 1$. After implementing sequential SVD for $d - 1$ times, the remaining $B_d \in \mathbb{R}^{r_{d-1} \times n}$ is a matrix and we take it as the final core in the tensor-train representation since no more decomposition is required.

Naively, the computational cost from SVD in Algorithm 1 scales exponentially large as $O(dn^{d+1})$ in terms of dimensionality. However, for the density estimation problem, we can take advantage of the structure of \hat{c} as defined in (20) to achieve a fast implementation of Algorithm 1. We will use the next subsection to elaborate such fast implementation.

2.2.1 Fast implementation of TT-SVD

In this subsection, we present a fast implementation of Algorithm 1 with a complexity of $O(dN^2nr)$, which scales linearly with d and is therefore well-suited for high-dimensional cases. Notably, this efficient implementation introduces no additional approximations and produces the same TT output as the direct implementation in Algorithm 1.

The key of the fast implementation lies in fast calculations of SVD of B_j in Algorithm 1. Instead of performing SVD to B_j directly to get its left singular vectors as in Line 2 of Algorithm 1, we consider computing the eigenvectors of $B_j B_j^T$, which is a relatively small matrix of size $nr_{j-1} \times nr_{j-1}$. However, one concern is that the cost of forming $B_j B_j^T$ can in principle scale exponentially with dimensionality, since the column size of B_j is n^{d-j} as indicated by the thick leg in Figure 4. Fortunately, by using the structure of \hat{c} as shown in Figure 3, one can form $B_j B_j^T$ much more efficiently. This is shown in Line 2 of Algorithm 2, which summarizes the TT-SVD procedure that is implemented in a computationally feasible manner.

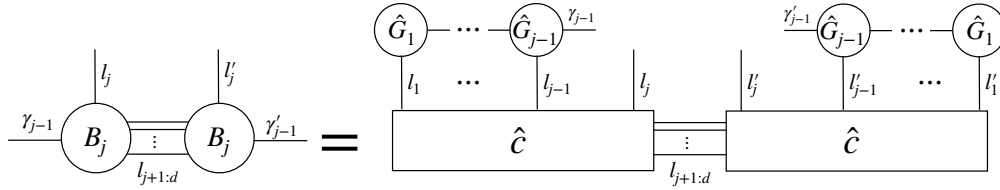


Figure 4: Tensor components for forming $B_j B_j^T$.

In Algorithm 2, the main computation lies in forming D_j and E_j in Line 2. A naive way is to compute them independently, leading to $O(dN^2)$ complexity. However, D_j and E_j can be computed in a recursive way efficiently, where computations can be reused. More precisely, one can precompute E_j by

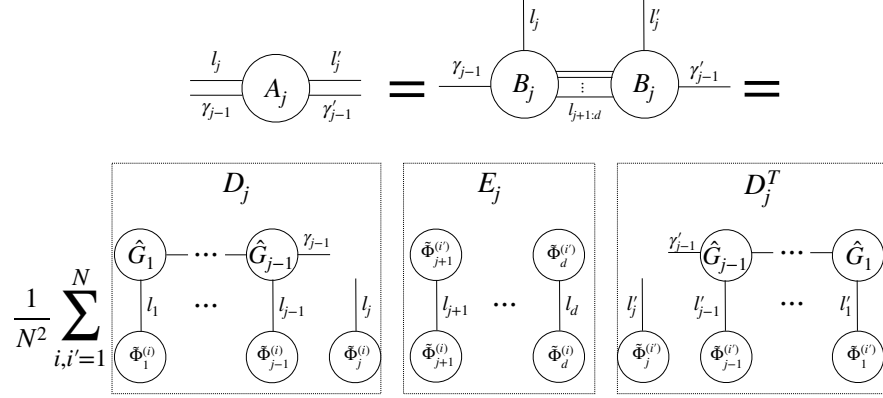
$$E_j = E_{j+1} \odot (\tilde{\Phi}_j \tilde{\Phi}_j^T) \quad (21)$$

starting from $E_d = I_{N \times N}$ which is $N \times N$ the identity matrix. Here \odot denotes the Hadamard (entrywise) product. D_j is computed recursively based on core \hat{G}_{j-1} starting from $D_1 = \tilde{\Phi}_1^T$ according to Figure 5. The last core \hat{G}_d is assigned as the matrix B_d in algorithm 1, which is equal to the average of $D_d^{(i)}$ over sample index i . Therefore, we compute \hat{G}_d as the average of $D_d^{(i)}$ in Algorithm 2. In this way, the computational cost of E_j , D_j and $B_j B_j^T$ is $O(N^2nr)$ which has no dependency on dimensionality. Afterwards, one can solve the core by eigen-decomposition of $B_j B_j^T \in \mathbb{R}^{nr_{j-1} \times nr_{j-1}}$ with a minor cost as $O((nr)^3)$. Overall, the computational cost of this fast implementation is $O(dN^2nr)$.

Algorithm 2 Fast implementation of TT-SVD

INPUT: Samples $\{x^{(i)}\}_{i=1}^N$. Target rank $\{r_1, \dots, r_{d-1}\}$.

- 1: **for** $j \in \{1, \dots, d-1\}$ **do**
- 2: Perform eigen-decomposition to $A_j := B_j B_j^T \in \mathbb{R}^{nr_{j-1} \times nr_{j-1}}$, which is computed by $A_j = \frac{1}{N^2} D_j E_j D_j^T$ where $D_j \in \mathbb{R}^{nr_{j-1} \times N}$ and $E_j \in \mathbb{R}^{N \times N}$ are the resulting matrices by contraction in the boxes of the below figure:



In particular, $D_1 = \tilde{\Phi}_1^T$ defined in (20). Here D_j and E_j should be computed recursively to reuse calculations. With eigen-decomposition $A_j = U_j \Lambda_j U_j^T$, we obtain the j -th core $\hat{G}_j \in \mathbb{R}^{r_{j-1} \times n \times r_j}$, which is reshaped from the first r_j principle eigenvectors in U_j .

- 3: **end for**
- 4: Obtain the last core:

$$\hat{G}_d = \frac{1}{N} \sum_{i=1}^N D_d^{(i)} \in \mathbb{R}^{r_{d-1} \times n}$$

where $D_d^{(i)}$ is the reshaping of i -th column of D_d .

OUTPUT: Tensor train $\tilde{c} = \hat{G}_1 \circ \hat{G}_2 \circ \dots \circ \hat{G}_d \in \mathbb{R}^{n \times n \times \dots \times n}$.

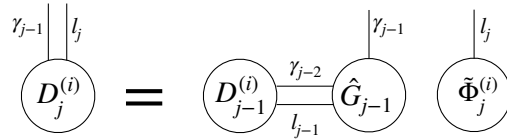


Figure 5: Tensor diagram illustrating the recursive calculation of $D_j^{(i)}$, which is the i -th column of the matrix D_j in Algorithm 2.

While this fast implementation significantly reduces the computational complexity from exponential to linear in d , we point out that such implementation still requires $O(N^2)$ computations to form each E_j , which can make it challenging with a large number of samples even in low dimensional cases. In Section 3, we will further improve Algorithm 2 using kernel Nyström approximation, which will bring computational cost to $O(dN)$ only.

2.3 Implementation of deconvolution

We now finish the last step of the main approach by implementing deconvolution and obtaining density estimator \tilde{p} in tensor-train format. As we have received the tensor-train coefficient \tilde{c} from the previous section, the deconvolution step is then done by

$$\tilde{p} = \Phi \text{diag}(\alpha)^{-1} \tilde{c}. \quad (22)$$

The structure of \tilde{p} is illustrated in Figure 6. Since \tilde{c} is a low-rank tensor train, the complexity of the evaluation on a single point x is only $O(dn)$.

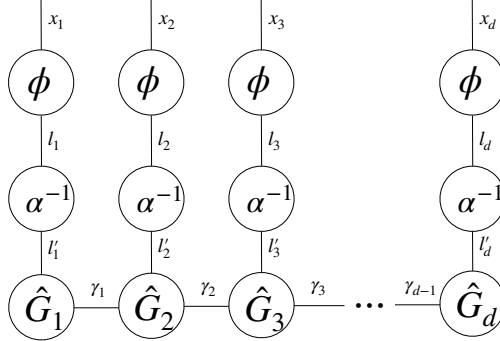


Figure 6: Tensor diagram for \tilde{p} .

Remark 1. *In practice, as dimensionality d grows, some elements in $\text{diag}(\alpha)$ become exponentially small, which potentially lead to instability when computing the inverse. One solution is to implement inverse with given threshold: $\tilde{p} = \Phi(\text{diag}(\alpha) + \lambda I)^{-1} \tilde{c}$. Here λ is a small thresholding constant to avoid instability issues and I is identity matrix. In practice, we find that even without this post-procedure, the tensor-train estimator does not suffer from such an instability.*

3 TT-SVD with kernel Nyström approximation (TT-SVD-kn)

In this section, we propose a further modification based on the fast implementation of TT-SVD developed in Section 2.2.1. This modification accelerates Algorithm 2 using kernel Nyström approximation to reduce the complexity from $O(dN^2)$ to $O(dN)$. As we have pointed out at the end of Section 2.2.1, the $O(N^2)$ complexity of Algorithm 2 is the consequence of exact evaluation of the $N \times N$ matrix E_j in the step of eigen-decomposition for $B_j B_j^T$. The proposed modification in this section will utilize kernel Nyström approximation (Williams and Seeger (2000)) to form E_j efficiently.

To begin with, we briefly introduce the idea of kernel Nyström method to approximate a symmetric matrix as shown in Figure 7. Given a symmetric matrix $A \in \mathbb{R}^{m \times m}$, the kernel Nyström method chooses \tilde{r} columns of A uniformly at random without replacement and approximates A by the following low-rank cross approximation

$$A \approx MW^+M^T \quad (23)$$

where $M \in \mathbb{R}^{m \times \tilde{r}}$ consists of the \tilde{r} chosen columns, $W \in \mathbb{R}^{\tilde{r} \times \tilde{r}}$ is the intersection of the chosen \tilde{r} columns and the corresponding \tilde{r} rows and W^+ is the Moore-Penrose generalized inverse of W .

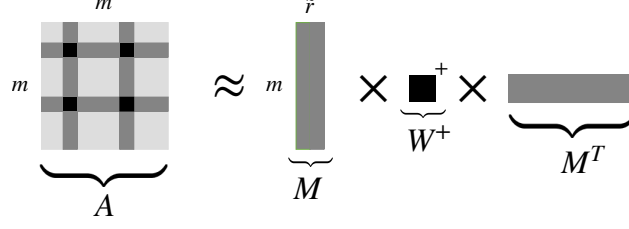


Figure 7: Cross approximation of a symmetric matrix.

Such approximation can be applied to the symmetric matrix E_j in Algorithm 2, resulting in the more efficient TT-SVD-kn algorithm summarized in Algorithm 3. By the recurrence relation (21), E_j is formulated as

$$E_j = (\tilde{\Phi}_d \tilde{\Phi}_d^T) \odot (\tilde{\Phi}_{d-1} \tilde{\Phi}_{d-1}^T) \odot \cdots \odot (\tilde{\Phi}_{j+1} \tilde{\Phi}_{j+1}^T), \quad (24)$$

which is depicted by the first equation in Figure 8. To apply kernel Nyström method, we randomly sample \tilde{r} rows in E_j with index $\mathcal{I} \subset \{1, 2, \dots, N\}$, and we define $\tilde{\Phi}_m^{(\mathcal{I})} \in \mathbb{R}^{\tilde{r} \times n}$, which is denoted by the blocks in each $\tilde{\Phi}_m$ in Figure 8, as the resulting submatrices formed by the sampled rows.

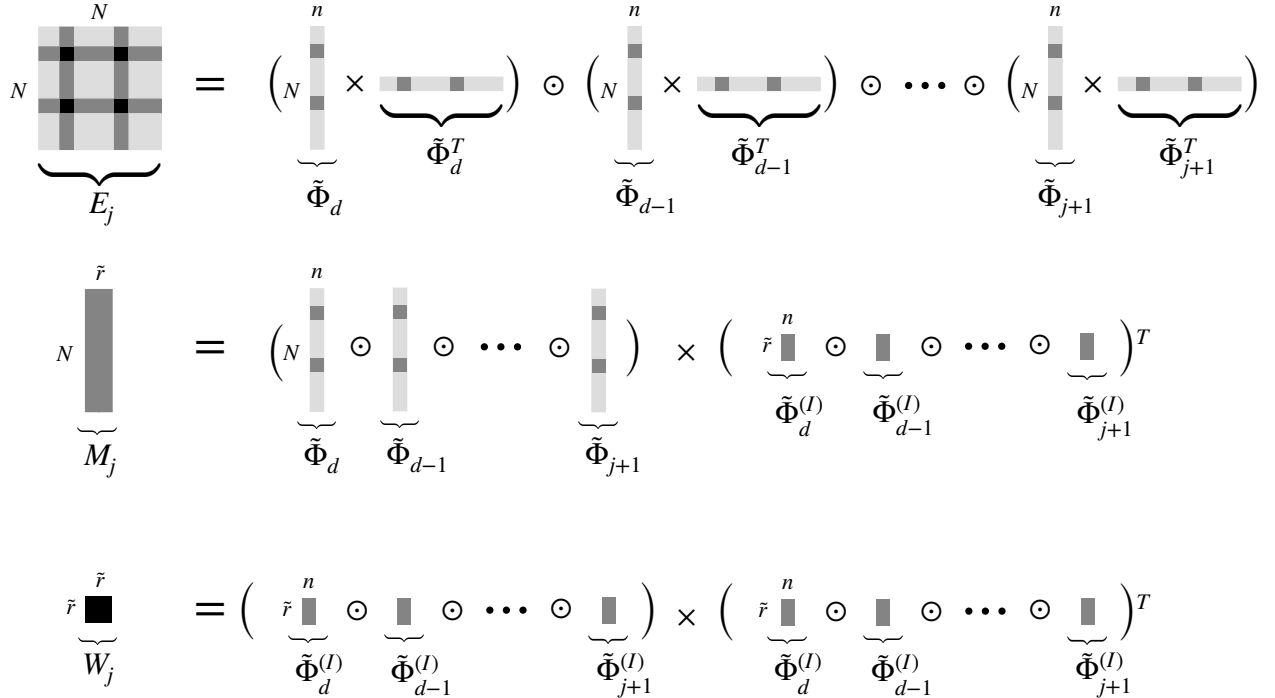


Figure 8: Cross approximation of E_j , the most expensive component in Algorithm 2.

At this point, we perform the cross approximation for E_j :

$$E_j \approx M_j W_j^+ M_j^T$$

where $M_j \in \mathbb{R}^{N \times \tilde{r}}$ is the submatrix formed by the chosen columns in E_j and $W_j \in \mathbb{R}^{\tilde{r} \times \tilde{r}}$ is the corresponding intersection. Using the expression (24), M_j and W_j are respectively formulated as

the second and third equation in Figure 8. The structures of M_j and W_j allow us to compute them in a recursive manner as in Line 2 of Algorithm 3: suppose we have already obtained $\tilde{\Phi}_{j+2:d}$ and $\tilde{\Phi}_{j+2:d}^{(\mathcal{I})}$, M_j and W_j can be evaluated with complexity $O(Nn)$ (direct computations based on their definitions in Figure 8 is $O(dNn)$). Consequently, $B_j B_j^T$ in the previous Algorithm 2 can now be approximated by

$$B_j B_j^T = \frac{1}{N^2} D_j E_j D_j^T \approx \frac{1}{N^2} D_j M_j W_j^+ M_j^T D_j^T$$

as in Line 4 of Algorithm 3. The computational cost for the above matrix multiplications is $O(Nnr \max(nr, \tilde{r}))$, which is significantly smaller compared to the original $O(N^2 nr)$ complexity in Algorithm 2. By considering the calculations for all d tensor cores, the total computational cost is $O(dNnr \max(nr, \tilde{r}))$. Here we remark that we have employed the same indices \mathcal{I} for computing all E_j . Such practice is the key to reuse the calculations in this recursive implementation so that we can achieve a complexity that is only linear in sample size.

Algorithm 3 TT-SVD-kn

INPUT: Samples $\{x^{(i)}\}_{i=1}^N$. Target rank $\{r_1, \dots, r_{d-1}\}$. Number of sampled columns \tilde{r} .

- 1: Sample \tilde{r} integers from $\{1, \dots, N\}$ and let \mathcal{I} be the set of sampled integers.
- 2: Pre-compute $\{W_j\}_{j=1}^{d-1}$ and $\{M_j\}_{j=1}^{d-1}$ based on sampled indices \mathcal{I} recursively by Figure 8.
- 3: **for** $j \in \{1, \dots, d-1\}$ **do**
- 4: Perform eigen-decomposition to $B_j B_j^T \in \mathbb{R}^{nr_{j-1} \times nr_{j-1}}$, which is approximated by

$$B_j B_j^T \approx A_j := \frac{1}{N^2} D_j M_j W_j^+ M_j^T D_j^T$$

where D_j is computed recursively as Figure 5. With eigen-decomposition $A_j = U_j \Lambda_j U_j^T$, we obtain the j -th core $\hat{G}_j \in \mathbb{R}^{r_{j-1} \times n \times r_j}$, which is reshaped from the first r_j principle eigenvectors in U_j .

- 5: **end for**
- 6: Obtain the last core:

$$\hat{G}_d = \frac{1}{N} \sum_{i=1}^N D_d^{(i)} \in \mathbb{R}^{r_{d-1} \times n}$$

where $D_d^{(i)}$ is the i -th column of D_d .

OUTPUT: Tensor train $\tilde{c} = \hat{G}_1 \circ \hat{G}_2 \circ \dots \circ \hat{G}_d \in \mathbb{R}^{n \times n \times \dots \times n}$.

4 TT-SVD with truncated cluster basis (TT-SVD-c)

In this section, we introduce the TT-SVD-c algorithm (Algorithm 4), which is a modified TT-SVD algorithm based on truncated cluster basis. The central idea is to utilize sketching technique to approximate the full SVDs of $B_j \in \mathbb{R}^{nr_{j-1} \times n^{d-j}}$ in Line 2 of Algorithm 1. More specifically, each step when we compute the left singular vectors U_j from B_j in Algorithm 1, we instead compute the left singular vectors from a sketched B_j :

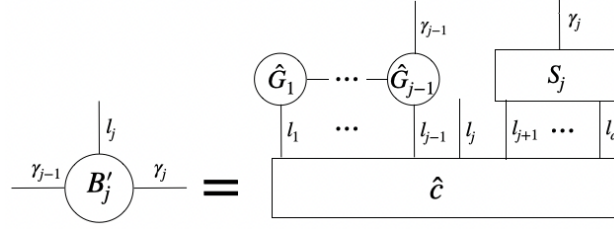
$$B'_j = B_j S_j, \tag{25}$$

where S_j is some appropriately chosen sketching matrix with size $n^{d-j} \times \tilde{r}_j$, with sketching size \tilde{r}_j much smaller than n^{d-j} (Line 2 of Algorithm 4). In this way, we can reduce the exponential complexity of full SVD for B_j to $O(\max(nr\tilde{r}_j^2, n^2r^2\tilde{r}_j))$ complexity of SVD for B'_j .

Algorithm 4 TT-SVD-c

INPUT: Samples $\{x^{(i)}\}_{i=1}^N$. Target rank $\{r_1, \dots, r_{d-1}\}$. Cluster order k .

- 1: **for** $j \in \{1, \dots, d-1\}$ **do**
- 2: Perform SVD to $B'_j \in \mathbb{R}^{nr_{j-1} \times \tilde{r}_j}$, which is formed by the following tensor contraction



The contraction of the righ-hand side is done efficiently as shown in Figure 9. With SVD $B'_j = U_j \Sigma_j V_j^T$, we obtain the j -th core $\hat{G}_j \in \mathbb{R}^{r_{j-1} \times n \times r_j}$, which is reshaped from the first r_j principle left singular vectors in U_j .

- 3: **end for**

4: Obtain the last core $\hat{G}_d = B'_d \in \mathbb{R}^{r_{d-1} \times n}$.

OUTPUT: Tensor train $\tilde{c} = \hat{G}_1 \circ \hat{G}_2 \circ \dots \circ \hat{G}_d \in \mathbb{R}^{n \times n \times \dots \times n}$.

To key of this approach is to choose good sketching matrix S_j such that B'_j retains the same range, and thus the same left singular space, as B_j . Here, we follow a specific way to construct sketching matrix S_j , where we only include the low-order cluster basis (Chen and Khoo (2023); Peng et al. (2023)). According to the choice of eigenvalues $\{\alpha_l\}_{l=1}^n$ in (19), each entry of high-dimensional tensor $\hat{c} \in \mathbb{R}^{n \times n \times \dots \times n}$ can be rewritten as

$$\hat{c}(l_1, l_2, \dots, l_d) = \frac{1}{N} \sum_{i=1}^N \alpha_{l_1} \alpha_{l_2} \dots \alpha_{l_d} \phi_{l_1}(x_1^{(i)}) \phi_{l_2}(x_2^{(i)}) \dots \phi_{l_d}(x_d^{(i)}).$$

Here the coefficient $\alpha_{l_1} \alpha_{l_2} \dots \alpha_{l_d}$ in the sum above takes the form α^m for $m = 0, 1, \dots, d$, where m is the number of l_j that are not 1. For convenience, we denote the set of indices l with m non-one l_j (called m -cluster index) by

$$\mathcal{B}^{m,d} = \{l \in [n]^d \mid \text{support of } (l_1 - 1, l_2 - 1, \dots, l_d - 1) \text{ has cardinality } m\}.$$

The cardinality of this set is $|\mathcal{B}^{m,d}| = \binom{d}{m} (n-1)^m$. In addition, when $m \geq d$, $\mathcal{B}^{m,d}$ includes all cluster indices.

Our choice of sketching matrix is based on the low-order cluster index. To sketch B_j , we construct $S_j \in \mathbb{R}^{n^{d-j} \times \tilde{r}_j}$ as follows: each column of S_j is an indicator vector corresponding to a multivariate index $l \in \bigcup_{m=0}^k \mathcal{B}^{m,d-j}$ where the cluster order k is chosen to be small. The indicator vector evaluates as 1 only on the support of $(l_1 - 1, l_2 - 1, \dots, l_{d-j} - 1)$ and evaluates as 0 elsewhere. Under this construction, S_j is a sparse matrix with column size $\tilde{r}_j = \sum_{m=0}^k |\mathcal{B}^{m,d-j}| = O(d^k n^k)$.

At this point, the only concern is that forming $B'_j = B_j S_j$ has exponential complexity by direct matrix multiplication. Similar to Algorithm 2, we utilize the structure of \hat{c} (20):

$$B'_j = B_j S_j = \frac{1}{N} D_j (E_j)^T = \frac{1}{N} \sum_{i=1}^N D_j^{(i)} (E_j^{(i)})^T \in \mathbb{R}^{nr_{j-1} \times \tilde{r}_j} \quad (26)$$

where D_j, E_j are defined in Figure 9 (c) and $D_j^{(i)}, E_j^{(i)}$ represent the i -th column of matrix D_j, E_j , respectively. According to the structure of D_j, E_j , their computation can be done in a recursive way following the diagram in Figure 9 (a) and (b).

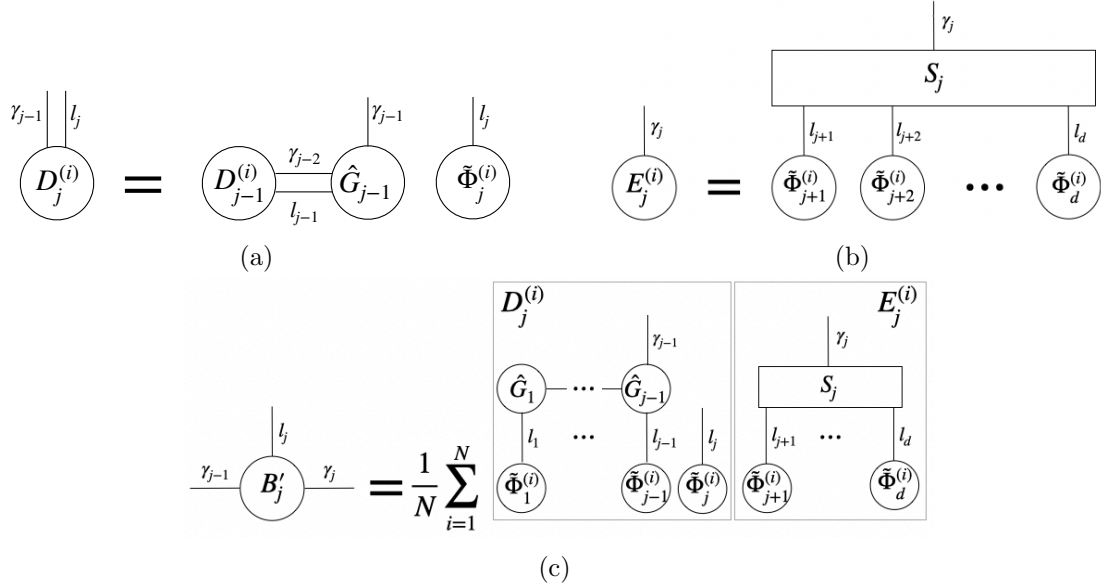


Figure 9: Tensor diagrams illustrating recursive computation of B'_j in Line 2 of Algorithm 4. (a) recursive calculation of $D_j^{(i)}$, which is the i -th column of the matrix D_j ; (b) recursive calculation of $E_j^{(i)}$, which is the i -th column of the matrix E_j ; (c) calculation of B'_j based on $D_j^{(i)}$ and $E_j^{(i)}$.

In terms of the computational complexity of Algorithm 4, the cost for $\{E_j\}_{j=1}^{d-1}$ is $O(d^{k+1} N n^k)$ for k -cluster truncation. Besides, the cost for $\{D_j\}_{j=1}^{d-1}$ follows the analysis in Figure 5 and Algorithm 2, which is $O(d N n r^2)$. Furthermore, the computational complexity of multiplication in B'_j and the following SVD step requires $O(d^{k+1} N n^{k+1})$. To summarize, the dominant term in computational complexity is $O(d^{k+1} N n^{k+1})$. The reduction is from standard TT-SVD algorithm $O(\min(d n^{d+1}, d N^2 n))$ to $O(d^{k+1} N n^{k+1})$, which is significant especially for a large sample size N and low-order k . In the following subsection, we further propose a modification of TT-SVD-c which constructs sketching matrix S_j based on hierarchical matrix decomposition. This acceleration can achieve a lower computational complexity as $O(d \log(d))$.

4.1 Acceleration of TT-SVD-c via hierarchical matrix decomposition

In this subsection, we propose a modification that further accelerates TT-SVD-c method with cluster order $k = 1$. The key insight of this acceleration lies in the assumption that the ground truth

density p^* has high correlations between nearby variables (such as x_1 and x_2) and low correlation between distant variables (such as x_1 and x_d), which is satisfied by many real cases. In Algorithm 4, the sketching matrix S_j considers all correlations equally without taking the distance into account, which includes redundant correlations with distant variables and leads to a large column size of S_j . In fact, even if cluster order $k = 1$, the column size is $O(d)$, which results in the overall computational cost of $O(d^2)$. This motivates us to further sketch S_j , which is done by hierarchical matrix decomposition (Hackbusch (1999); Hackbusch and Khoromskij (2000); Bebendorf (2008)) of covariance matrix M , whose (j_1, j_2) -block is formulated as

$$M_{j_1, j_2} = [\mathbb{E}_{\tilde{p}}[\phi_{l_1}(x_{j_1})\phi_{l_2}(x_{j_2})]]_{l_1, l_2} \in \mathbb{R}^{n \times n} \quad (27)$$

for all $1 \leq j_1, j_2 \leq d$.

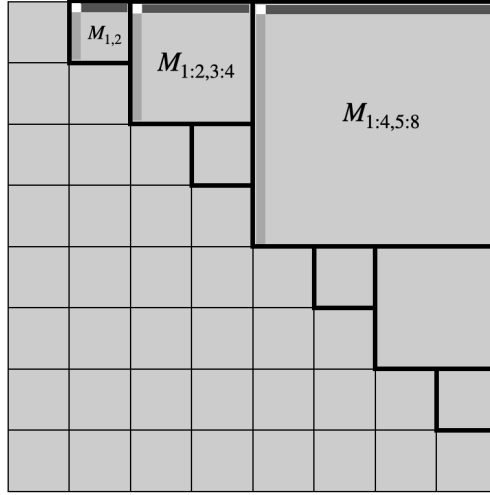


Figure 10: Hierarchical matrix decomposition of covariance matrix for $d = 8$. The figure depicts the three block matrices $M_{1:4,5:8}$, $M_{1:2,3:4}$, $M_{1,2}$ whose top \tilde{r} right singular vectors (visualized as dark grey matrix in each block matrix).

To illustrate the idea, we consider an example with $d = 8$. Covariance matrix M is depicted in Figure 10, where we use $M_{j_1:j_2, j_3:j_4}$ to represent the submatrix formed by blocks with row index from j_1 to j_2 and column index from j_3 to j_4 . To implement hierarchical matrix decomposition, we perform SVD on upper triangular off-diagonal blocks $M_{1:4,5:8}$, $M_{1:2,3:4}$, $M_{1,2}$ and get top \tilde{r} right singular vectors V'_1, V'_2, V'_3 , respectively. Here the sketching size \tilde{r} (different from that in Algorithm 4) is chosen as a constant. V'_1, V'_2, V'_3 respectively capture correlations with variables $x_{5:8}$, $x_{3:4}$ and x_2 .

Once the singular vectors V'_1, V'_2, V'_3 are obtained, we can use them to construct sketching matrices with smaller column sizes. When computing the first core \hat{G}_1 , we form $Q_1 = \text{diag}[V'_1, V'_2, V'_3] \in \mathbb{R}^{7n \times 3\tilde{r}}$ which captures the weighted correlation between x_1 and $x_{2:8}$, and we use S_1 and Q_1 to sketch B_1 as $B'_1 = B_1 S_1 Q_1 \in \mathbb{R}^{n \times 3\tilde{r}}$. Once this is done, we perform SVD to B'_1 to obtain \hat{G}_1 . For the second core, we form $Q_2 = \text{diag}[V'_1, V'_2] \in \mathbb{R}^{6n \times 2\tilde{r}}$ to capture the weighted correlation between variables x_2 and variables $x_{3:8}$. Then we sketch $B'_2 = B_2 S_2 Q_2$, and perform SVD to B'_2 to obtain \hat{G}_2 . Note that we can reuse V'_1, V'_2 in the second step since both of them were already computed in the first step. By repeating the procedure and generating new sketch $B'_j = B_j S_j Q_j$ for the remaining j , this hierarchical approach enables the efficient computation of all cores $\{\hat{G}_j\}_{j=1}^d$.

In terms of computational complexity, there are two major sources of computations. The first is the SVD of off-diagonal block matrices ($M_{1:4,5:8}, M_{1:2,3:4}, M_{1,2}$ for $d = 8$). For each block, we first apply kernel Nyström approximation (23) with \tilde{r} sampled rows and columns, followed by SVD. The cost for this part of computations is $O(d \log(d) N n \tilde{r})$. The second major computation is forming $B'_j = B_j S_j Q_j$. The number of columns in the weight matrix Q_j is at most $\log_2(d) \tilde{r}$. Since S_j is a sparse matrix, the computation of $B'_j = B_j S_j Q_j$ for all j needs $O(d \log(d) N n \tilde{r})$ computational cost upon leveraging a similar strategy for computing (26). The computational costs discussed above are the dominant cost in Algorithm 4. We can replace S_j with $S_j Q_j$ in Algorithm 4 and follow the operations in Figure 9, the method achieves a reduced computational complexity $O(d \log(d) N n)$ compared to the original complexity $O(d^2 N n^2)$ for TT-SVD-c with cluster order $k = 1$.

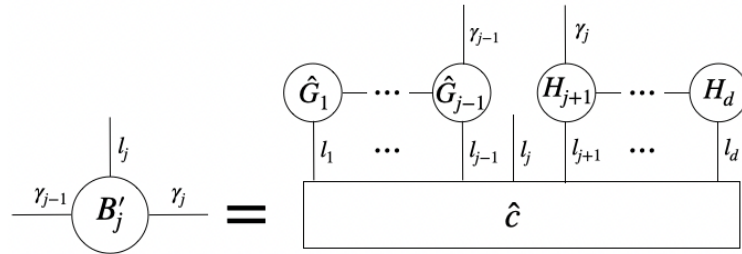
5 TT-SVD with random tensorized sketching (TT-rSVD-t)

In this section, we propose another modification for TT-SVD algorithm via sketching. This approach follows the randomized sketching technique (Huber et al. (2017)), originated from randomized linear algebra literature (Halko et al. (2011)), to accelerate SVD. The key idea is to choose sketching matrix $S_j \in \mathbb{R}^{n^{d-j} \times \tilde{r}}$ as some random matrix, where \tilde{r} is a given sketching size, which is usually chosen to be reasonably larger than target rank r of the output tensor-train estimator. Afterwards, similar as TT-SVD-c, we perform SVD to $B'_j = B_j S_j$. In general, the matrix multiplication $B_j S_j$ has exponentially large computational cost. Our solution to this curse of dimensionality is to form S_j by a set of random tensor trains, leading to the TT-rSVD-t algorithm summarized in Algorithm 5.

Algorithm 5 TT-rSVD-t

INPUT: Samples $\{x^{(i)}\}_{i=1}^N$. Target rank $\{r_1, \dots, r_{d-1}\}$. Sketching size \tilde{r} .

- 1: Generate random tensor train with cores $\{H_j\}_{j=1}^d$, where $H_1 \in \mathbb{R}^{n \times \tilde{r}}, H_2, \dots, H_{d-1} \in \mathbb{R}^{\tilde{r} \times n \times \tilde{r}}, H_d \in \mathbb{R}^{\tilde{r} \times n}$.
- 2: **for** $j \in \{1, \dots, d-1\}$ **do**
- 3: Perform SVD to $B'_j \in \mathbb{R}^{n r_{j-1} \times \tilde{r}_j}$, which is formed by the following tensor contraction



The contraction of the right-hand side is done efficiently as shown in Figure 11. With SVD $B'_j = U_j \Sigma_j V_j^T$, we obtain the j -th core $\hat{G}_j \in \mathbb{R}^{r_{j-1} \times n \times r_j}$, which is reshaped from the first r_j principle left singular vectors in U_j .

4: **end for**

5: Obtain the last core $\hat{G}_d = B'_d \in \mathbb{R}^{r_{d-1} \times n}$.

OUTPUT: Tensor train $\hat{c} = \hat{G}_1 \circ \hat{G}_2 \circ \dots \circ \hat{G}_d \in \mathbb{R}^{n \times n \times \dots \times n}$.

To implement Algorithm 5, we first generate a d -dimensional random tensor train with fixed rank \tilde{r} whose cores are H_1, H_2, \dots, H_d (Line 1). In practice, we can set each core as i.i.d. random Gaussian matrix/tensor or random uniform matrix/tensor. When sketching B_j , we construct sketching matrix $S_j \in \mathbb{R}^{n^{d-j} \times \tilde{r}}$ as the reshaping of $H_{j+1} \circ H_{j+2} \circ \dots \circ H_d$ (Line 3). Afterwards, we contract B_j with S_j and perform SVD to solve the j -th core \hat{G}_j .

Similar to (26) for TT-SVD-c, B'_j is computed recursively as illustrated in Figure 11(c). The key difference lies in the new formulation of E_j , which arises from the new choice of sketching matrix S_j . Leveraging the tensor-train structure, E_j can also be computed recursively as shown in Figure 11(b). The total computational cost for $\{E_j\}_{j=1}^{d-1}$ is $O(dNn\tilde{r}^2)$. The computation of $\{D_j\}_{j=1}^{d-1}$, depicted in Figure 11(a), follows the same approach used in Algorithm 2 and incurs a computational cost of $O(dNn\tilde{r}^2)$. Overall, the SVD step required to compute all tensor cores has a total complexity of $O(dNn\tilde{r}^2)$, which is linear with respect to both dimensionality and sample size.

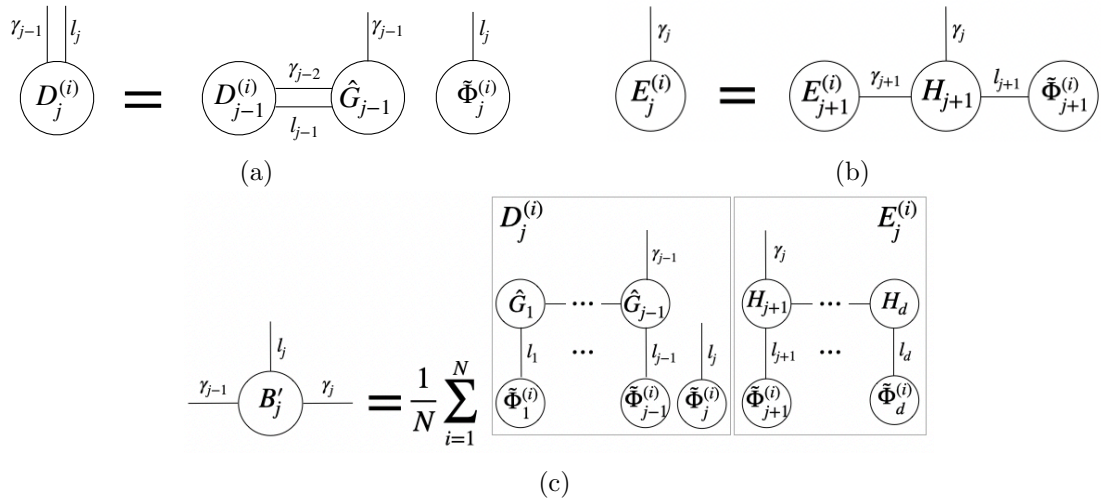


Figure 11: Tensor diagrams illustrating recursive computation of B'_j in Line 2 of Algorithm 5. (a) recursive calculation of $D_j^{(i)}$, which is the i -th column of the matrix D_j ; (b) recursive calculation of $E_j^{(i)}$, which is the i -th column of the matrix E_j ; (c) calculation of B'_j based on $D_j^{(i)}$ and $E_j^{(i)}$.

At this point, we have introduced all tensor compression algorithms in this work. We summarize the computational complexity of these methods in Table 1, which will later be verified by the numerical experiments in the subsequent section.

Algorithm	Computational Complexity
TT-SVD	$O(\min(dn^{d+1}, dN^2n))$
TT-SVD-kn	$O(dNn)$
TT-SVD-c (k -cluster)	$O(d^{k+1}Nn^{k+1})$
TT-SVD-c (hierarchical)	$O(d \log(d)Nn)$
TT-rSVD-t	$O(dNn)$

Table 1: Computational complexity of proposed methods.

6 Numerical results

In this section, we carry out numerical experiments to examine the performance of our proposed density estimation algorithms. In specific, we use TT-SVD-kn (Algorithm 3), TT-SVD-c (Algorithm 4) with hierarchical matrix decomposition and TT-rSVD-t (Algorithm 5). Throughout this section, we set the number of sampled columns in Nyström approximation $\tilde{r} = 100$ in TT-SVD-kn, sketching size $\tilde{r} = 10$ in TT-SVD-c with hierarchical matrix decomposition, sketching size $\tilde{r} = 30$ in TT-rSVD-t and the kernel parameter $\alpha = 0.01$. The choice of these parameters are empirical.

6.1 Gaussian mixture model

We first consider the d -dimensional Gaussian mixture model which is defined as :

$$\frac{1}{6}\mathcal{M}(0.18) + \frac{1}{3}\mathcal{M}(0.2) + \frac{1}{2}\mathcal{M}(0.22)$$

where

$$\mathcal{M}(\sigma) = \frac{2}{3}\mathcal{N}(-0.5, \sigma^2 I_{d \times d}) + \frac{1}{3}\mathcal{N}(0.5, \sigma^2 I_{d \times d}).$$

We set the domain as the hypercube $[-L, L]^d$ where $L = 1.5$ with mesh size 0.1 in each direction.

We first fix dimension $d = 10$. We draw N i.i.d samples from the mixture model, and use proposed three algorithms to fit a TT approximation for the empirical distribution of these samples. For the algorithms, we set fixed target rank $r = 3$ and use the Fourier basis

$$\phi_k(x) = \begin{cases} \frac{1}{\sqrt{2L}}, & \text{for } k = 0, \\ \frac{1}{\sqrt{L}} \cos\left(\frac{k\pi x}{2L}\right) & \text{for even } k > 0 \\ \frac{1}{\sqrt{L}} \sin\left(\frac{(k+1)\pi x}{2L}\right) & \text{for odd } k > 0 \end{cases} \quad (28)$$

for $k = 0, \dots, n$ with $n = 15$ as the univariate orthonormal basis function. In the left panel of Figure 12, we test different sample number N and plot the L_2 relative error defined by

$$\|\tilde{p} - p^*\|_{L_2} / \|p^*\|_{L_2}$$

in logarithm scale. One can observe that the relative error decays with Monte Carlo rate $O(1/\sqrt{N})$.

Next, we fix the sample size $N = 10^6$ and test our algorithms with various dimensions d . The L_2 relative error is plotted in right panel of Figure 12, which exhibits sublinear growth with increasing dimensionality according to the curves. In particular, with $N = 10^6$ samples, our algorithms can achieve two-digit L_2 relative error up to $d = 12$. For dimensionality higher than that, we can expect that the error can also be controlled below 0.1 for a sufficiently large sample size, as suggested by the Monte Carlo convergence observed in the previous experiment.

Finally, we verify the time complexity of the algorithms. In Figure 13, we plot the wall clock time of three algorithms for fixed $d = 5$ with various N (left panel) and fixed $N = 10000$ with various d (right panel). The rates of wall clock time verify the theoretical computational complexity at listed in Table 1.

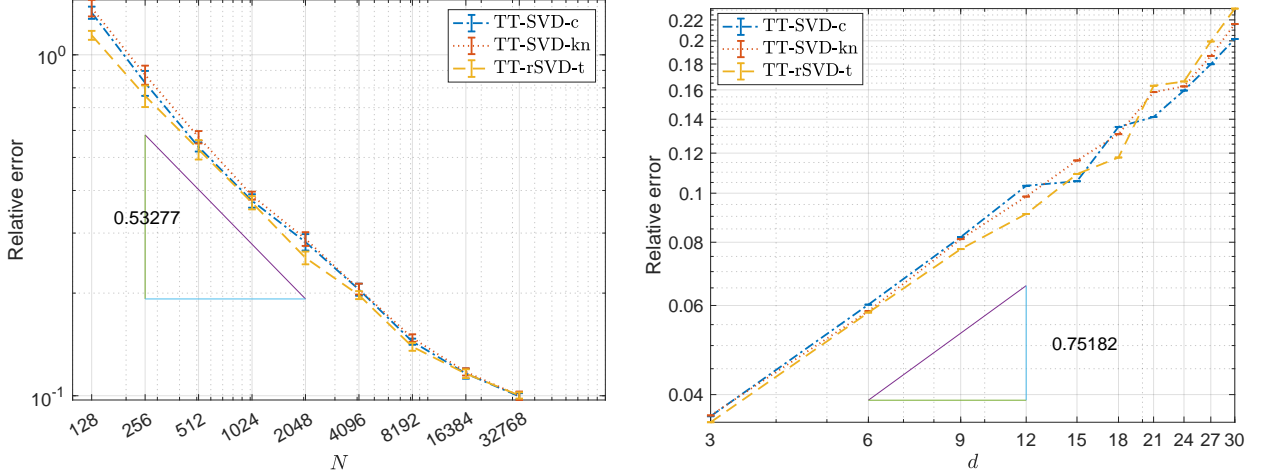


Figure 12: Gaussian mixture model: L_2 relative error for proposed algorithms (we apply hierarchical matrix decomposition for TT-SVD-c). Left: $d = 10$ and sample number $N = 2^7, 2^8, \dots, 2^{15}$. Right: $N = 10^6$ and dimension $d = 3, 6, 9, \dots, 30$.

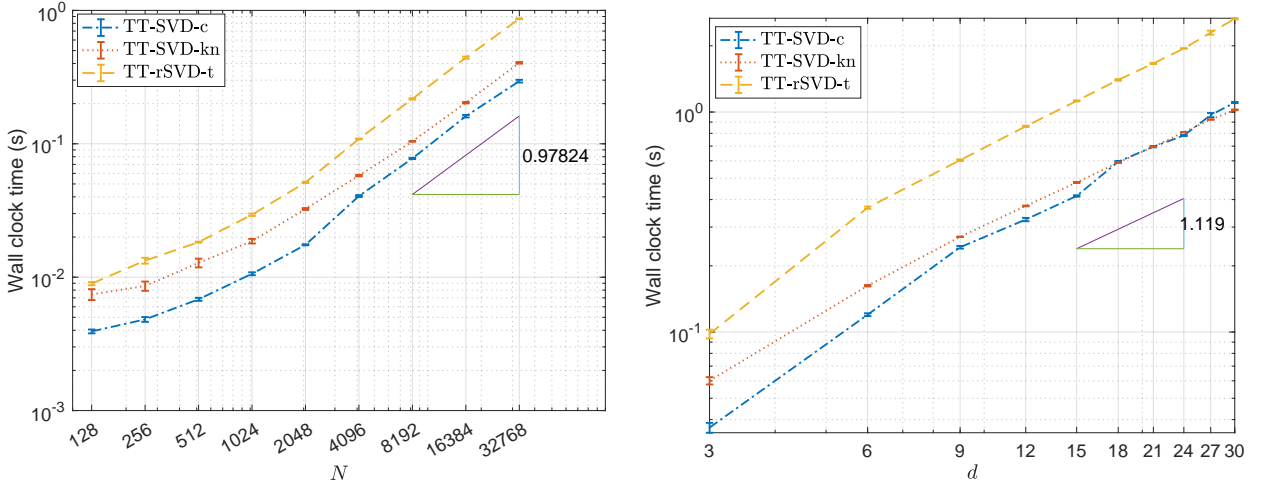


Figure 13: Gaussian mixture model: average wall clock time (seconds) for proposed algorithms (we apply hierarchical matrix decomposition for TT-SVD-c). Left: $d = 5$ and sample number $N = 2^7, 2^8, \dots, 2^{15}$. Right: $N = 10000$ and dimension $d = 3, 6, 9, \dots, 30$.

6.2 Ginzburg-Landau model

Now we consider a more practical problem in statistical physics as the Ginzburg-Landau model [Hoffmann and Tang \(2012\)](#). In particular, we consider the density estimation for the Boltzmann distribution $p^*(x) = \frac{1}{Z}e^{-\beta V(x)}$ where β is the inverse temperature, Z is the normalization factor such that $\int p^*(x)dx = 1$, and V is the Ginzburg-Landau potential energy.

6.2.1 1D Ginzburg-Landau model

We first consider a 1D Ginzburg-Landau model where the potential energy is formulated as

$$V(x_1, \dots, x_d) = \sum_{i=1}^{d+1} \frac{\lambda}{2} \left(\frac{x_i - x_{i-1}}{h} \right)^2 + \frac{1}{4\lambda} (1 - x_i^2)^2 \text{ for } x \in [-L, L]^d \quad (29)$$

where $x_0 = x_{d+1} = 0$, $h = 1/(1+d)$, $\lambda = 0.03$ and $\beta = 1/8$. We consider hypercube domain $[-L, L]^d$ with $L = 2.5$ and mesh size 0.05 in each direction. For the ground truth p^* , we use DMRG-cross algorithm to get p^* in TT form. The samples of p^* are generated by running Langevin dynamics for sufficiently long time.

In Table 2, we list the L_2 relative error of the approximated densities estimated by $N = 10^6$ samples with different number of univariate basis functions. For this example, we set fixed target rank $r = 4$. One can observe that the approximation improves as we use more basis functions. Such improvement can be further visualized in Figure 14, where we plot the marginal distribution of the approximated solutions solved by three algorithms when $d = 20$. All of them give accurate match to the sample histograms when a sufficient number of basis functions are used.

n	$d = 5$			$d = 10$		
	TT-SVD-c	TT-SVD-kn	TT-rSVD-t	TT-SVD-c	TT-SVD-kn	TT-rSVD-t
7	0.2810	0.2809	0.2810	0.4304	0.4304	0.4305
11	0.0782	0.0781	0.0781	0.1365	0.1365	0.1378
15	0.0305	0.0304	0.0301	0.0488	0.0483	0.0533
19	0.0275	0.0273	0.0289	0.0449	0.0404	0.0526
n	$d = 15$			$d = 20$		
	TT-SVD-c	TT-SVD-kn	TT-rSVD-t	TT-SVD-c	TT-SVD-kn	TT-rSVD-t
7	0.6342	0.6342	0.6343	0.7897	0.7897	0.7898
11	0.2169	0.2167	0.2186	0.3017	0.3016	0.3037
15	0.0733	0.0740	0.0836	0.1126	0.1125	0.1158
19	0.0613	0.0602	0.0716	0.0884	0.0874	0.1099

Table 2: 1D G-L model: comparison of L_2 relative errors with $N = 10^6$ and $d = 5, 10, 15, 20$ under different numbers of univariate basis functions used.

6.2.2 2D Ginzburg-Landau model

Next, we consider the 2D Ginzburg-Landau model which is defined on a $m \times m$ lattice. The potential energy is formulated as

$$V(x_{1,1}, \dots, x_{m,m}) = \frac{\lambda}{2} \sum_{i=1}^{m+1} \sum_{j=1}^{m+1} \left[\left(\frac{x_{i,j} - x_{i-1,j}}{h} \right)^2 + \left(\frac{x_{i,j} - x_{i,j-1}}{h} \right)^2 \right] + \frac{1}{4\lambda} \sum_{i=1}^m \sum_{j=1}^m (1 - x_{i,j}^2)^2$$

with the boundary condition

$$x_{0,j} = x_{m+1,j} = 1, \quad x_{i,0} = x_{i,m+1} = -1 \quad \forall i, j = 1, \dots, m$$

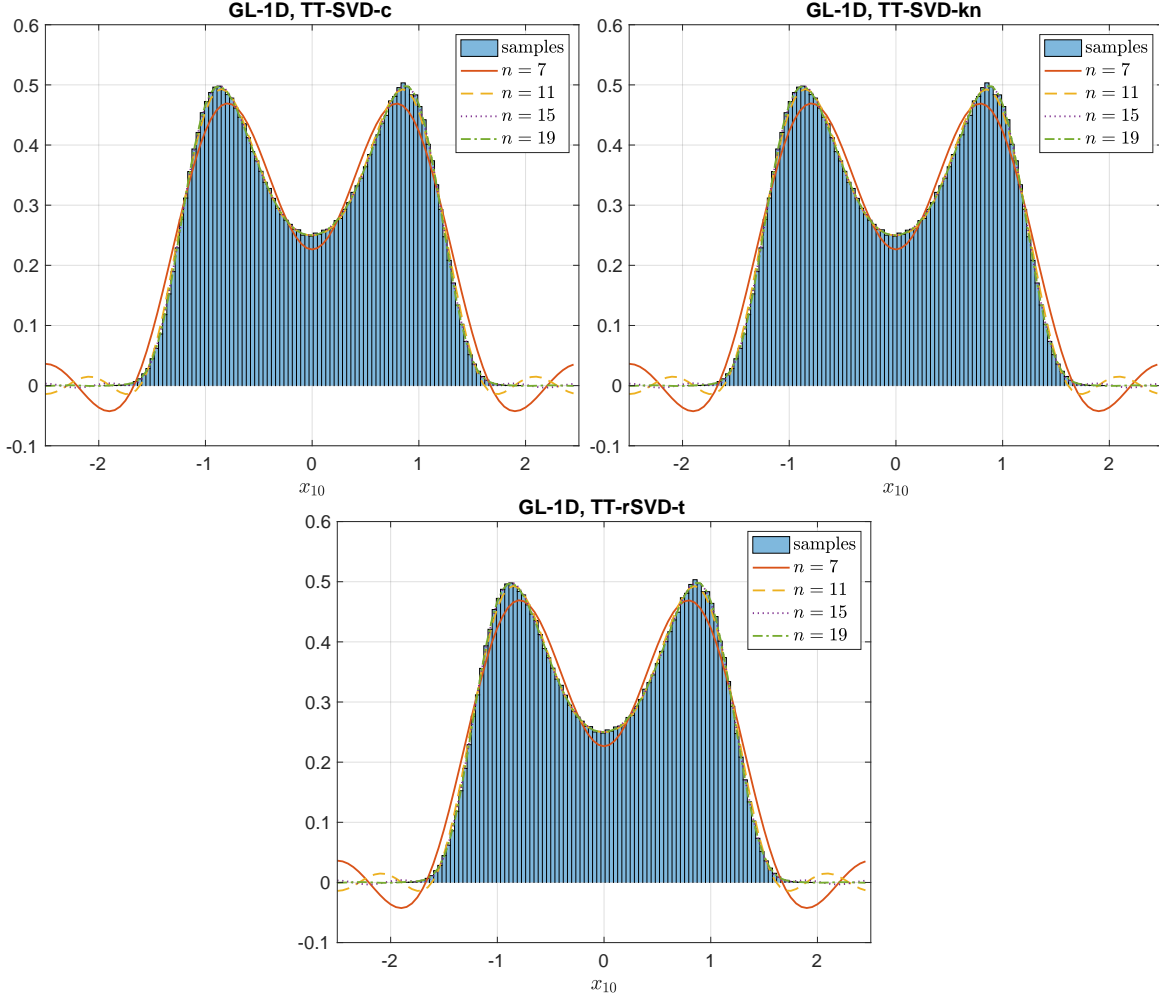


Figure 14: 1D G-L model: x_{10} -marginal of approximated solutions for $d = 20$ and $N = 10^6$ under different numbers of univariate basis functions used.

where we choose parameter $h = 1/(1 + m)$, $\lambda = 0.03$ and inverse temperature $\beta = 1/3$. We set $L = 2.5$ with mesh size 0.05 for the domain. We consider a test example where $m = 8$ and thus the total number of dimensionality is $m^2 = 64$. In this 2D model, we apply a space-filling curve [Sagan \(2012\)](#) to order the dimensions as shown in [Figure 15](#), and our fitted TT will have the same ordering. For the algorithms, we set target rank $r = 6$ and we use $N = 10^5$ samples and $n = 21$ Fourier basis.

In this section, we evaluate the performance of our fitted tensor-train densities as generative models. Specifically, we use $N = 10^5$ samples as training data to learn densities in tensor-train format using our proposed algorithms. Subsequently, we generate another $N = 10^5$ samples as testing data from these estimated densities via TT conditional sampling [Dolgov et al. \(2020\)](#), which operates in linear time. [Figure 16](#) illustrates the $(x_{4,4}, x_{5,5})$ -marginal and $(x_{7,2}, x_{8,6})$ -marginal distributions of the generated samples. For comparison, we also show results for 10^6 reference samples drawn directly from the Boltzmann distribution using Langevin dynamics, as well as results from a neural network ([Papamakarios et al. \(2017\)](#)) using the same $N = 10^5$ training data size.

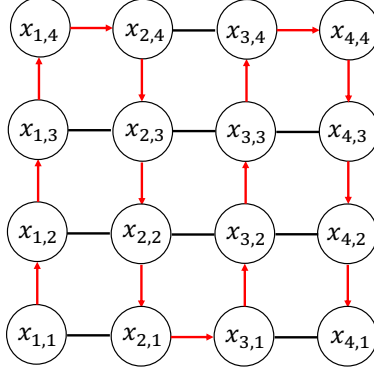


Figure 15: 2D G-L model: ordering of the variables $x_{i,j}$ on a 4×4 lattice.

The visualizations reveal that samples generated from tensor trains capture local minima more accurately and align better with the reference sample histograms, compared to the neural network approach. To quantify this difference, we compute the L_2 relative error of two-marginal distributions against the reference. The errors are summarized in Table 3.

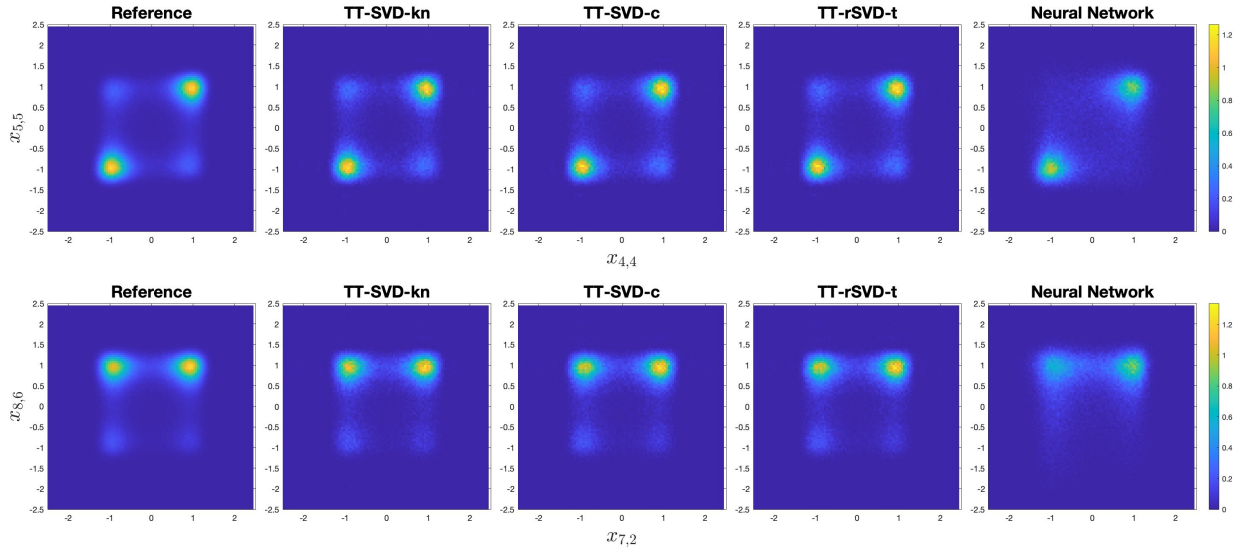


Figure 16: 2D G-L model on a 8×8 lattice: visualization of $(x_{4,4}, x_{5,5})$ -marginal (first row) and $(x_{7,2}, x_{8,6})$ -marginal (second row). Left to right: reference sample histograms, samples from tensor trains fitted by proposed algorithms, and samples from neural network for comparison.

7 Conclusion

In this paper, we propose a new distance metric for high-dimensional density, which allows the construction of a density estimator as a low-rank functional tensor train. To this end, we provide four tensor decomposition algorithms. The first one is based on direct TT-SVD algorithm with fast implementation in a density estimation setting. The second algorithm follows a Nystöm

Marginal	TT-SVD-kn	TT-SVD-c	TT-rSVD-t	NN
$(x_{4,4}, x_{5,5})$	0.1013	0.0967	0.1103	0.2095
$(x_{7,2}, x_{8,6})$	0.0876	0.0914	0.0963	0.2351

Table 3: 2D G-L model on a 8×8 lattice: L_2 relative errors of $(x_{4,4}, x_{5,5})$ -marginal and $(x_{7,2}, x_{8,6})$ -marginal under proposed algorithms, and neural network for comparison.

approximation. The third approach modifies the first approach by thresholding certain elements in the tensor and employing a hierarchical matrix factorization to accelerate the computational efficiency. The last algorithm employs a tensorized sketching technique. Several of these proposed algorithms can achieve computational complexity that is linear both in dimensionality d and sample size N . Comprehensive numerical experiments validate the accuracy of all proposed algorithms, in comparison to other density estimators. While this work focuses on practical implementations, a rigorous theoretical analysis of the numerical methods will be explored in future research.

References

- Charu C Aggarwal, Alexander Hinneburg, and Daniel A Keim. On the surprising behavior of distance metrics in high dimensional space. In *Database theory—ICDT 2001: 8th international conference London, UK, January 4–6, 2001 proceedings 8*, pages 420–434. Springer, 2001.
- Markus Bachmayr, Reinhold Schneider, and André Uschmajew. Tensor networks and hierarchical tensors for the solution of high-dimensional partial differential equations. *Foundations of Computational Mathematics*, 16:1423–1472, 2016.
- Mario Bebendorf. *Hierarchical matrices*. Springer, 2008.
- Tai-Danae Bradley, E Miles Stoudenmire, and John Terilla. Modeling sequences with quantum states: a look under the hood. *Machine Learning: Science and Technology*, 1(3):035008, 2020.
- Kamalika Chaudhuri, Sanjoy Dasgupta, Samory Kpotufe, and Ulrike Von Luxburg. Consistent procedures for cluster tree estimation and pruning. *IEEE Transactions on Information Theory*, 60(12):7900–7912, 2014.
- Yen-Chi Chen. A tutorial on kernel density estimation and recent advances. *Biostatistics & Epidemiology*, 1(1):161–187, 2017.
- Yian Chen and Yuehaw Khoo. Combining particle and tensor-network methods for partial differential equations via sketching. *arXiv preprint arXiv:2305.17884*, 2023.
- Kyle Cranmer. Kernel estimation in high-energy physics. *Computer Physics Communications*, 136(3):198–207, 2001.
- Richard A Davis, Keh-Shin Lii, and Dimitris N Politis. Remarks on some nonparametric estimates of a density function. *Selected Works of Murray Rosenblatt*, pages 95–100, 2011.
- Laurent Dinh, David Krueger, and Yoshua Bengio. Nice: Non-linear independent components estimation. *arXiv preprint arXiv:1410.8516*, 2014.

- Laurent Dinh, Jascha Sohl-Dickstein, and Samy Bengio. Density estimation using real nvp. *arXiv preprint arXiv:1605.08803*, 2016.
- Sergey Dolgov, Karim Anaya-Izquierdo, Colin Fox, and Robert Scheichl. Approximation and sampling of multivariate probability distributions in the tensor train decomposition. *Statistics and Computing*, 30:603–625, 2020.
- Yilun Du and Igor Mordatch. Implicit generation and modeling with energy based models. *Advances in Neural Information Processing Systems*, 32, 2019.
- Mathieu Germain, Karol Gregor, Iain Murray, and Hugo Larochelle. Made: Masked autoencoder for distribution estimation. In *International conference on machine learning*, pages 881–889. PMLR, 2015.
- Ian Goodfellow, Jean Pouget-Abadie, Mehdi Mirza, Bing Xu, David Warde-Farley, Sherjil Ozair, Aaron Courville, and Yoshua Bengio. Generative adversarial networks. *Communications of the ACM*, 63(11):139–144, 2020.
- Wolfgang Hackbusch. A sparse matrix arithmetic based on-matrices. part i: Introduction to-matrices. *Computing*, 62(2):89–108, 1999.
- Wolfgang Hackbusch and Boris N Khoromskij. A sparse h-matrix arithmetic. part ii: Application to multi-dimensional problems. *Computing*, 64:21–47, 2000.
- Nathan Halko, Per-Gunnar Martinsson, and Joel A Tropp. Finding structure with randomness: Probabilistic algorithms for constructing approximate matrix decompositions. *SIAM review*, 53(2):217–288, 2011.
- Zhao-Yu Han, Jun Wang, Heng Fan, Lei Wang, and Pan Zhang. Unsupervised generative modeling using matrix product states. *Physical Review X*, 8(3):031012, 2018.
- Karl-Heinz Hoffmann and Qi Tang. *Ginzburg-Landau Phase Transition Theory and Superconductivity*. Birkhäuser Basel, 2012.
- Benjamin Huber, Reinhold Schneider, and Sebastian Wolf. A randomized tensor train singular value decomposition. In *Compressed Sensing and its Applications: Second International MATHEON Conference 2015*, pages 261–290. Springer, 2017.
- William Huggins, Piyush Patil, Bradley Mitchell, K Birgitta Whaley, and E Miles Stoudenmire. Towards quantum machine learning with tensor networks. *Quantum Science and technology*, 4(2):024001, 2019.
- Yoonhaeng Hur, Jeremy G Hoskins, Michael Lindsey, E Miles Stoudenmire, and Yuehaw Khoo. Generative modeling via tensor train sketching. *Applied and Computational Harmonic Analysis*, 67:101575, 2023.
- Yuehaw Khoo, Yifan Peng, and Daren Wang. Nonparametric estimation via variance-reduced sketching. *arXiv preprint arXiv:2401.11646*, 2024.
- Taesup Kim and Yoshua Bengio. Deep directed generative models with energy-based probability estimation. *arXiv preprint arXiv:1606.03439*, 2016.

- Daniel Kressner and André Uschmajew. On low-rank approximability of solutions to high-dimensional operator equations and eigenvalue problems. *Linear Algebra and its Applications*, 493:556–572, 2016.
- Daniel Kressner, Bart Vandereycken, and Rik Voorhaar. Streaming tensor train approximation. *SIAM Journal on Scientific Computing*, 45(5):A2610–A2631, 2023.
- Ji Liu, Przemyslaw Musialski, Peter Wonka, and Jieping Ye. Tensor completion for estimating missing values in visual data. *IEEE transactions on pattern analysis and machine intelligence*, 35(1):208–220, 2012.
- Qiao Liu, Jiase Xu, Rui Jiang, and Wing Hung Wong. Density estimation using deep generative neural networks. *Proceedings of the National Academy of Sciences*, 118(15):e2101344118, 2021.
- YP Mack and Murray Rosenblatt. Multivariate k-nearest neighbor density estimates. *Journal of Multivariate Analysis*, 9(1):1–15, 1979.
- Jay Mardia, Jiantao Jiao, Ervin Tánčzos, Robert D Nowak, and Tsachy Weissman. Concentration inequalities for the empirical distribution of discrete distributions: beyond the method of types. *Information and Inference: A Journal of the IMA*, 9(4):813–850, 2020.
- Jonathan Niles-Weed and Philippe Rigollet. Estimation of wasserstein distances in the spiked transport model. *Bernoulli*, 28(4):2663–2688, 2022.
- Georgii S Novikov, Maxim E Panov, and Ivan V Oseledets. Tensor-train density estimation. In *Uncertainty in artificial intelligence*, pages 1321–1331. PMLR, 2021.
- Ivan Oseledets and Eugene Tyrtyshnikov. Tt-cross approximation for multidimensional arrays. *Linear Algebra and its Applications*, 432(1):70–88, 2010.
- Ivan V Oseledets. Tensor-train decomposition. *SIAM Journal on Scientific Computing*, 33(5):2295–2317, 2011.
- George Papamakarios, Theo Pavlakou, and Iain Murray. Masked autoregressive flow for density estimation. *Advances in neural information processing systems*, 30, 2017.
- Emanuel Parzen. On estimation of a probability density function and mode. *The annals of mathematical statistics*, 33(3):1065–1076, 1962.
- Yifan Peng, Yian Chen, E Miles Stoudenmire, and Yuehaw Khoo. Generative modeling via hierarchical tensor sketching. *arXiv preprint arXiv:2304.05305*, 2023.
- David Perez-Garcia, Frank Verstraete, Michael M Wolf, and J Ignacio Cirac. Matrix product state representations. *arXiv preprint quant-ph/0608197*, 2006.
- Danilo Rezende and Shakir Mohamed. Variational inference with normalizing flows. In *International conference on machine learning*, pages 1530–1538. PMLR, 2015.
- Hans Sagan. *Space-filling curves*. Springer Science & Business Media, 2012.

- Dmitry Savostyanov and Ivan Oseledets. Fast adaptive interpolation of multi-dimensional arrays in tensor train format. In *The 2011 International Workshop on Multidimensional (nD) Systems*, pages 1–8. IEEE, 2011.
- David W Scott. On optimal and data-based histograms. *Biometrika*, 66(3):605–610, 1979.
- David W Scott. Averaged shifted histograms: effective nonparametric density estimators in several dimensions. *The Annals of Statistics*, pages 1024–1040, 1985.
- Richik Sengupta, Soumik Adhikary, Ivan Oseledets, and Jacob Biamonte. Tensor networks in machine learning. *European Mathematical Society Magazine*, (126):4–12, 2022.
- Tianyi Shi, Maximilian Ruth, and Alex Townsend. Parallel algorithms for computing the tensor-train decomposition. *SIAM Journal on Scientific Computing*, 45(3):C101–C130, 2023.
- Qingquan Song, Hancheng Ge, James Caverlee, and Xia Hu. Tensor completion algorithms in big data analytics. *ACM Transactions on Knowledge Discovery from Data (TKDD)*, 13(1):1–48, 2019.
- Yang Song and Stefano Ermon. Generative modeling by estimating gradients of the data distribution. *Advances in neural information processing systems*, 32, 2019.
- Edwin Stoudenmire and David J Schwab. Supervised learning with tensor networks. *Advances in neural information processing systems*, 29, 2016.
- Yiming Sun, Yang Guo, Charlene Luo, Joel Tropp, and Madeleine Udell. Low-rank tucker approximation of a tensor from streaming data. *SIAM Journal on Mathematics of Data Science*, 2(4):1123–1150, 2020.
- Xun Tang and Lexing Ying. Solving high-dimensional fokker-planck equation with functional hierarchical tensor. *arXiv preprint arXiv:2312.07455*, 2023.
- Xun Tang, Yoonhaeng Hur, Yuehaw Khoo, and Lexing Ying. Generative modeling via tree tensor network states. *arXiv preprint arXiv:2209.01341*, 2022.
- Benigno Uribe, Marc-Alexandre Côté, Karol Gregor, Iain Murray, and Hugo Larochelle. Neural autoregressive distribution estimation. *The Journal of Machine Learning Research*, 17(1):7184–7220, 2016.
- Jonathan Weed and Francis Bach. Sharp asymptotic and finite-sample rates of convergence of empirical measures in wasserstein distance. 2019.
- Steven R White. Density-matrix algorithms for quantum renormalization groups. *Physical review b*, 48(14):10345, 1993.
- Christopher Williams and Matthias Seeger. Using the nyström method to speed up kernel machines. *Advances in neural information processing systems*, 13, 2000.
- Adriano Z Zambom and Ronaldo Dias. A review of kernel density estimation with applications to econometrics. *International Econometric Review*, 5(1):20–42, 2013.